



Fermi-LAT Detection of the Low-luminosity Radio Galaxy NGC 4278 during the LHAASO Campaign

Ettore Bronzini^{1,2} , Paola Grandi³ , Eleonora Torresi³ , and Sara Buson^{4,5}

¹ Dipartimento di Fisica e Astronomia “Augusto Righi,” Università di Bologna, via P. Gobetti 93/2, 40129 Bologna, Italy; ettore.bronzini@inaf.it

² INAF, Astrophysics and Space Science Observatory Bologna, via P. Gobetti 93/3, 40129 Bologna, Italy

³ INAF, Astrophysics and Space Science Observatory Bologna, via P. Gobetti 101, 40129 Bologna, Italy

⁴ Julius-Maximilians-Universität Würzburg, Fakultät für Physik und Astronomie, Emil-Fischer-Str. 31, D-97074 Würzburg, Germany

⁵ DESY, D-15738 Zeuthen, Germany

Received 2024 September 24; revised 2024 November 12; accepted 2024 November 14; published 2024 December 3

Abstract

We present a study of the high-energy properties of the compact symmetric object NGC 4278, recently associated with a TeV source by the Large High Altitude Air Shower Observatory (LHAASO) collaboration. We conducted a dedicated analysis of a Fermi Large Area Telescope (LAT) region around NGC 4278, limited to the LHAASO campaign conducted from 2021 March to 2022 October. A statistically significant emission ($\sim 4.3\sigma$) was revealed, spatially consistent with the radio position of NGC 4278 and the LHAASO source. The Fermi-LAT source is detected above 8 GeV, exhibiting a hard spectrum (photon index $\Gamma = 1.3 \pm 0.3$) and a γ -ray luminosity of $L_{>100 \text{ MeV}} \simeq 4 \times 10^{41} \text{ erg s}^{-1}$. A serendipitous Swift X-Ray Telescope (XRT) observation of NGC 4278 during the TeV campaign reveals the source in a high state, with a flux $F_{0.5-8 \text{ keV}} = 5_{-2}^{+3} \times 10^{-12} \text{ erg s}^{-1} \text{ cm}^{-2}$, compatible with the highest luminosity level observed in previous Chandra pointings. The high-energy spectral energy distribution of the source and the intense flux variation observed in the X-ray band support a jet origin for the observed radiation. We suggest that the significant enhancement of the high-energy flux observed during the LHAASO campaign is due to a transient, highly energetic perturbation in the jet. The detection of NGC 4278 at both high and very high energies opens new frontiers in studying particle acceleration processes. It reveals that even compact, low-power radio galaxies can exceed the sensitivity thresholds of GeV and TeV instruments, becoming promising targets for the upcoming Cherenkov Telescope Array Observatory.

Unified Astronomy Thesaurus concepts: Gamma-rays (637); X-ray active galactic nuclei (2035); Low-luminosity active galactic nuclei (2033); Relativistic jets (1390)

1. Introduction

In the past three decades, very long baseline interferometry imaging surveys (e.g., P. N. Wilkinson et al. 1994; A. B. Peck & G. B. Taylor 2000) have revealed the presence of compact radio sources hosted at the center of many massive galaxies. Among these small, barely resolved objects, compact symmetric objects (CSOs) are characterized by radio emission on both sides of an active galactic nucleus (AGN), linear sizes less than 1 kpc (P. N. Wilkinson et al. 1994), low variability, low apparent speeds along the jets (S. Kiehlmann et al. 2024), and kinematic ages smaller than a few thousand years (M. Orienti 2016).

In the radio band, CSOs are characterized by convex synchrotron spectra, peaking at $\sim 1 \text{ GHz}$ (C. P. O’Dea & S. A. Baum 1997; M. Orienti 2016; C. P. O’Dea & D. J. Saikia 2021). This spectral characteristic is interpreted in terms of absorption mechanisms, with the emission being optically thin (thick) above (below) the peak frequency (see I. A. G. Snellen et al. 2000; M. Orienti & D. Dallacasa 2008; J. R. Callingham et al. 2015; S. J. Tingay et al. 2015 for further details).

The nature and compactness of CSOs are still a matter of debate. The following scenarios are among those proposed to explain their peculiar properties: (i) the youth scenario, which suggests that the radio activity has been triggered recently for the first time ($\lesssim 100 \text{ yr}$; C. Fanti et al. 1995; I. Owsianik &

J. E. Conway 1998; I. Owsianik et al. 1998; W. Tschager et al. 2000); (ii) they might be confined by an extraordinarily dense interstellar medium (ISM) of the host galaxies (e.g., W. van Breugel et al. 1984; C. P. O’Dea et al. 1991; D. Dicken et al. 2012); (iii) they might be living an intermittent/transient phase of radio activity due to instabilities in the accretion disk (B. Czerny et al. 2009), to accretion of a limited amount of material (e.g., a star, A. C. S. Readhead et al. 1994), or to the disruption of the jet (e.g., D. S. De Young 1991; R. S. Sutherland & G. V. Bicknell 2007; A. Y. Wagner & G. V. Bicknell 2011; G. V. Bicknell et al. 2018; D. Mukherjee et al. 2018). In the case of recurrent activity, drops in surface brightness profiles and diffuse radio relics are expected on scales larger than the CSO size (e.g., S. A. Baum et al. 1990; G. B. Taylor et al. 1998; A. Marecki et al. 2003; C. Stanghellini 2003; H. L. Maness et al. 2004; C. Stanghellini et al. 2005). The central engine itself is old ($\gtrsim 10^4 \text{ yr}$; C. P. O’Dea & D. J. Saikia 2021, and references therein), but the components related to the CSO morphologies, hence the radio source, are young (\lesssim hundreds of years; e.g., I. A. G. Snellen et al. 2000).

Studies of CSOs at high energies are fundamental in tracing the most energetic processes in action in these sources. Few theoretical models predict γ -ray emission from CSOs from GeV up to TeV energies (Ł. Stawarz et al. 2008; H. Ito et al. 2011; M. Kino & K. Asano 2011; M. Kino et al. 2013; G. Migliori et al. 2014). At GeV energies, only three CSOs have been detected so far and included in the latest Fermi Large Area Telescope (LAT) Fourth Source Catalog—Data Release 4 (4FGL-DR4, J. Ballet et al. 2023): PKS 1718-649



Original content from this work may be used under the terms of the [Creative Commons Attribution 4.0 licence](https://creativecommons.org/licenses/by/4.0/). Any further distribution of this work must maintain attribution to the author(s) and the title of the work, journal citation and DOI.

(G. Migliori et al. 2016), NGC 3894 (G. Principe et al. 2020), and TXS 0128+554 (M. L. Lister et al. 2020). All sources show no statistically significant variability and are well described by a simple power-law model with a photon index of $\Gamma \gtrsim 2$ and luminosities in the 0.1–100 GeV band ranging from 10^{42} to 10^{47} erg s $^{-1}$. None of them has been detected above 100 GeV to date.

The association of the Large High Altitude Air Shower Observatory (LHAASO; Z. Cao et al. 2019) source 1LHAASO J1219+2915 with the CSO NGC 4278 (Z. Cao et al. 2024a, 2024b) represents a remarkable discovery, opening new opportunities to investigate particle acceleration processes in low-luminosity radio galaxies still confined within their host galaxies. In this Letter, we present a detailed study of NGC 4278 with Fermi-LAT data simultaneous to the first LHAASO campaign (from 2021 March to 2022 October), reporting a γ -ray detection of the source at a significance of $\sim 4.3\sigma$. Furthermore, we show that, during the same period, the X-ray core of the source was in a high state, suggesting significant activity in the nuclear region of NGC 4278. Throughout this work, a flat cosmology with $H_0 = 67.4$ km s $^{-1}$ Mpc $^{-1}$ and $\Omega_m = 0.315$ (Planck Collaboration et al. 2020) is adopted.

2. NGC 4278

NGC 4278 is a nearby ($D_L \simeq 16.4$ Mpc; J. L. Tonry et al. 2001) early-type galaxy, part of a small group (A. M. Garcia 1993), with no evidence of interaction with the lower-mass companion galaxy NGC 4283. The nuclear region of NGC 4278 hosts a low-luminosity AGN ($M_{\text{SMBH}} \simeq 3 \times 10^8 M_\odot$; T.-G. Wang & X.-G. Zhang 2003; M. Chiaberge et al. 2005), powered by a radiatively inefficient accretion flow (L. C. Ho et al. 1997; B. Balmaverde & A. Capetti 2014). NGC 4278 is the faintest and most compact source among the known CSOs (S. Kiehlmann et al. 2024; A. C. S. Readhead et al. 2024).

Very Long Baseline Array (P. J. Napier et al. 1994) observations both at 5 and 8.4 GHz revealed a two-sided radio emission, with a spectral index of $\alpha \gtrsim 0.54$,⁶ and emerging from a dominant, flat-spectrum core ($\alpha \sim 0$; M. Giroletti et al. 2005; S. E. Tremblay et al. 2016). The overall radio spectrum, which peaks roughly at 1 GHz (M. Giroletti et al. 2005; S. E. Tremblay et al. 2016), is consistent with synchrotron radiation by accelerated relativistic particles (N. M. Nagar et al. 2002). The source shows variability in the radio band on yearly timescales, with an enhanced activity at 6 cm around 1985, while there is more quiescent activity from 1990 to 2005 (M. Giroletti et al. 2005). The edge-darkened FR I-like morphology, with a radio linear size of ~ 3 pc, suggests type I CSO characteristics (see S. E. Tremblay et al. 2016; A. C. S. Readhead et al. 2024 for further details). The estimated jet power of the source is modest ($L_{\text{jet}} \sim 10^{42}$ erg s $^{-1}$; see S. Pellegrini et al. 2012, hereafter P12, for details). The S-shaped symmetry observed, with the northern jet approaching us at a mildly relativistic speed ($\beta = v/c \sim 0.75$) and seen at an inclination angle between 2° and 4° (M. Giroletti et al. 2005), is peculiar, even if not unique for CSOs (e.g., S. A. Baum et al. 1990; A. C. S. Readhead et al. 1993; G. B. Taylor et al. 2009). The distorted radio morphology might be due to beaming effects or, alternatively, to the jet

interaction with the surrounding medium (M. Giroletti et al. 2005).

From IR to UV, the overall emission of NGC 4278 is dominated by the host galaxy and dust emission. Its stellar population is old (>10 Gyr) with no sign of ongoing star formation both in near-UV and mid-IR (H. Kuntschner et al. 2010; K. L. Shapiro et al. 2010). The nuclear emission is unresolved in the optical band (A. Capetti et al. 2000). G. Younes et al. (2010) detected optical nuclear variability up to a factor of 4 between 2006 December and 2007 January using the Hubble Space Telescope. In the UV band, the nucleus is barely resolved and rapidly variable (A. Cardullo et al. 2009), as commonly observed in most low-ionization nuclear emission-line region galaxies (D. Maoz et al. 2005): an enhanced flux by a factor of 1.6 was observed between 1994 June and 1995 January (A. Cardullo et al. 2009).

NGC 4278 has been extensively studied in the X-ray band with Chandra and XMM-Newton (L. C. Ho et al. 2001; Y. Terashima & A. S. Wilson 2003; O. González-Martín et al. 2009; G. Fabbiano et al. 2010; G. Younes et al. 2010; L. Hernández-García et al. 2013). Chandra images of NGC 4278 are dominated by the nuclear pointlike emission, whose best-fit model is a superposition of a power-law spectrum ($\Gamma = 2.31 \pm 0.20$) and a thermal component ($kT = (0.75 \pm 0.05)$ keV), with a low level of obscuration ($N_{\text{H}} = (4.2 \pm 3.1) \times 10^{20}$ cm $^{-2}$; P12). The nuclear emission shows a variability in Chandra images, with a luminosity of the power-law component in the range $L_{0.5-8 \text{ keV}} \simeq 0.3-6 \times 10^{40}$ erg s $^{-1}$.

At γ -ray energies, NGC 4278 is not reported in the latest 4FGL-DR4 catalog (J. Ballet et al. 2023), nor in the previous ones. It was revealed during a 1 month flare from 2009 March 5 to April 5 and is listed in the First Catalog of Long-term Transient Sources (1FLT; L. Baldini et al. 2021), based on the first 10 yr of Fermi-LAT data. On that occasion, the source was detected with a significance of about 5σ , a photon flux of $F_{0.1-300 \text{ GeV}} = (9.8 \pm 3.1) \times 10^{-8}$ ph s $^{-1}$ cm $^{-2}$, and a photon index of $\Gamma = 3.3 \pm 0.4$. However, the probability that this event is a false-positive detection is nonnegligible ($P \sim 34\%$; L. Baldini et al. 2021).

NGC 4278 has been suggested as a possible counterpart of 1LHAASO J1219+2915, a very-high-energy (VHE) γ -ray source detected by the LHAASO Water Cherenkov Detector Array (WCDA), and is listed in the first LHAASO catalog (Z. Cao et al. 2024a). This catalog was compiled using 508 days of data collected by the WCDA from 2021 March to 2022 September and 933 days of data recorded by the Kilometer Squared Array (KM2A) from 2020 January to 2022 September. However, we note that 1LHAASO J1219+2915 was not detected by KM2A; therefore, in the following, we will refer only to WCDA data. More recently, an extended study up to the end of 2023 October (Z. Cao et al. 2024b), leading to an effective livetime of about 891 days, was performed. A pointlike emission located at $\sim 0^\circ 03'$ (R.A. = $185^\circ 05' \pm 0^\circ 04'$, decl. = $29^\circ 25' \pm 0^\circ 03'$) from the radio position of NGC 4278 is detected at an overall significance of 6.1σ . Interestingly, the source showed hints of variability (p -value = 2.6×10^{-3}), with an enhanced TeV activity, from the middle of 2021 August to the middle of 2022 January, of about 7 times the low state (Z. Cao et al. 2024b). During the active phase, the source was detected at 7.8σ , and the spectrum is well described in the 1–15 TeV energy band by a single power-law model, with a photon index of $\Gamma = 2.56 \pm 0.14$ and a flux of

⁶ Here, spectral indices are defined such that $S(\nu) \propto \nu^{-\alpha}$, with $S(\nu)$ being the flux density.

$F_{1-10 \text{ TeV}} = (7.0 \pm 1.1_{\text{stat.}} \pm 0.4_{\text{syst.}}) \times 10^{-13} \text{ ph cm}^{-2} \text{ s}^{-1}$ (Z. Cao et al. 2024b). The proximity of NGC 4278 makes the $\gamma\gamma$ absorption due to the extragalactic background light negligible.

3. Fermi-LAT Analysis

The discovery of TeV photon emission in a very low luminosity radio galaxy has prompted the immediate question whether its emission may also extend to GeV energies and may be observable by Fermi-LAT. Our aim was twofold: (1) to corroborate the TeV detection and (2) to extend the spectral study to lower γ -ray energies in order to shed light on the physical processes at work.

The Fermi-LAT is a γ -ray telescope that detects photons by conversion into electron-positron pairs. Its operational energy range extends from $\sim 50 \text{ MeV}$ up to $\sim 1 \text{ TeV}$. The Fermi-LAT is equipped with a high-resolution converter tracker (for direct measurement of the incident γ -rays), a CsI(Tl) crystal calorimeter (for energy measurement), and an anticoincidence detector to reject the background of charged particles (W. B. Atwood et al. 2009).

Unlike other attempts to search for GeV signals from the source with Fermi-LAT recently reported in the literature (Z. Cao et al. 2024b; J.-S. Lian et al. 2024; Z.-R. Wang et al. 2024), our approach was to limit the investigation to the time interval corresponding to the first LHAASO catalog (Z. Cao et al. 2024a).

We inspected the Fermi-LAT region around NGC 4278, integrating data from 2021 March 1 (MJD = 59274) to 2022 October 1 (MJD = 59853). We considered both front- and back-converted events in the 100 MeV–1 TeV energy range. We selected the SOURCE class events and the P8R3_SOURCE_V3 instrument response functions (P. Bruel et al. 2018).

The data analysis was performed by exploiting the open-source python package *Fermipy* v.1.2.0 (M. Wood et al. 2017) with *Fermitools* v.2.2.0. Only good time intervals (LAT_CONFIG=1 and DATA_QUAL>0) were selected, resulting in an exposure time of $\sim 1.3 \text{ yr}$. We verified that the Sun and the Moon were at a distance greater than 20° from NGC 4278 and therefore do not affect our data.

Taking advantage of the event partition introduced with PASS 8 (W. Atwood et al. 2013), we analyzed separately the four different event classes, each characterized by its own point-spread function (PSF). Each PSF indicates the quality of the reconstructed direction of the event, from the best (PSF3) to the worst (PSF0). Following the procedure outlined in the 4FGL-DR3 catalog (S. Abdollahi et al. 2022), we further divided the data into six different energy bands. The number of bins and the optimal zenith angle selection remain consistent across each energy interval, while each event type necessitates a different pixel size depending on the PSF width (refer to Table 1 in S. Abdollahi et al. 2022). Differently from the 4FGL-DR3 catalog, we additionally split the 30 GeV–1 TeV energy bin into the four PSF components. In total, we dealt with 21 components.

A circular region of interest (RoI) of radius 15° centered on the radio position of NGC 4278 (R.A. = $185^\circ 02' 43.9''$, decl. = $29^\circ 28' 07.54''$; C. Ly et al. 2004) was chosen. The model included the most recent template for Galactic interstellar diffuse emission (gll_iem_v07.fits), the isotropic background components appropriate for each PSF (iso_P8R3_SOURCE_V3_PSFx_v1.txt),⁷ and the sources

listed in the 4FGL-DR4 catalog (J. Ballet et al. 2023). The energy dispersion correction (edisp_bins=-2) is enabled for all sources except the isotropic component. The test statistic (TS) was used to estimate the significance of a source.⁸ Preliminarily, a fast optimization of the entire RoI was performed, deriving the best-fit model of the RoI. As NGC 4278 is not included in the 4FGL-DR4 catalog, we included a point source at the radio coordinate position of the target and parameterized it with a power-law model with a spectral index initially fixed to 2. Then, the parameters of both diffuse components along with the spectral parameters of sources within a 5° radius surrounding the source of interest were set to vary during the fit. Only the normalizations were left free to vary for sources at a distance between 5° and 10° from the center of the RoI. The spectral parameters of sources at larger distances, as well as the faintest ones (TS < 4), were kept fixed. A binned likelihood fit, minimized using *Minuit*, was performed for all 21 components separately and then was summed to obtain the total log-likelihood. After performing the fit, we searched for the best position of the source detected at the center of the RoI. The peak of the emission was found at R.A. = $184^\circ 99'$ and decl. = $29^\circ 28'$, with a long and a short radius of error ellipse at 68% confidence of $\theta_{\text{maj.}} = 0^\circ 028'$ and $\theta_{\text{min.}} = 0^\circ 024'$ and a position angle of $\theta_{\text{p.a.}} = 58^\circ 5'$.

The significance of the source detection results in TS = 29. According to the Wilks' theorem (S. S. Wilks 1938), the distribution of the TS asymptotically approaches the χ^2 distribution under the null hypothesis $\mathcal{L}_{\text{null}}$ (W. Cash 1979). The p -value we measured, assuming a χ^2 distribution with 4 degrees of freedom, i.e., the two spectral parameters plus the coordinates, is $p\text{-value} \simeq 7.8 \times 10^{-6}$. This corresponds to a Gaussian significance for the detection of $\sim 4.3\sigma$.

NGC 4278 exhibits a hard photon index ($\Gamma = 1.3 \pm 0.3$) and an energy flux $F_{>100 \text{ MeV}} = (1.2 \pm 0.5) \times 10^{-11} \text{ erg s}^{-1} \text{ cm}^{-2}$ corresponding to an isotropic luminosity of $L_{>100 \text{ MeV}} = (4 \pm 2) \times 10^{41} \text{ erg s}^{-1}$. Given the hardness of the source, this flux is consistent to the flux above 1 GeV.

The resulting localization is shown in the TS map in Figure 1 that was generated using a power-law spectral model with a photon index of 2. The orange star marks the radio position of NGC 4278, while the violet and white stars are the LHAASO and Fermi-LAT best-fit positions, respectively. The LHAASO and Fermi-LAT 95% localization uncertainty regions are shown as dashed circular regions using the same color code.

To consolidate our analysis, we used the *gtsrcprob*⁹ tool to estimate the probability of each event to be associated with each source included in the input model. In particular, we adopted this tool to select events with the highest probability of being associated with NGC 4278. We observed that the detection is driven by three high-energy events, all front converted, with a probability of more than 90% of being associated with NGC 4278 (see column (6) in Table 1). Specifically, we detected one high-energy photon at 8.2 GeV and two VHE photons at 95.5 and 102.5 GeV, each having a probability exceeding 99%.

⁸ The TS corresponds to the logarithmic ratio of the likelihood of a model with the source being at a given position in a grid (\mathcal{L}_{src}) to the likelihood of the model without the source ($\mathcal{L}_{\text{null}}$), $\text{TS} = 2 \log(\mathcal{L}_{\text{src}}/\mathcal{L}_{\text{null}})$ (J. R. Mattox et al. 1996).

⁹ See https://raw.githubusercontent.com/fermi-lat/fermitools-fhelp/master/fhelp_files/gtsrcprob.txt for further details.

⁷ See <https://fermi.gsfc.nasa.gov/ssc/data/access/lat/BackgroundModels.html> for further details.

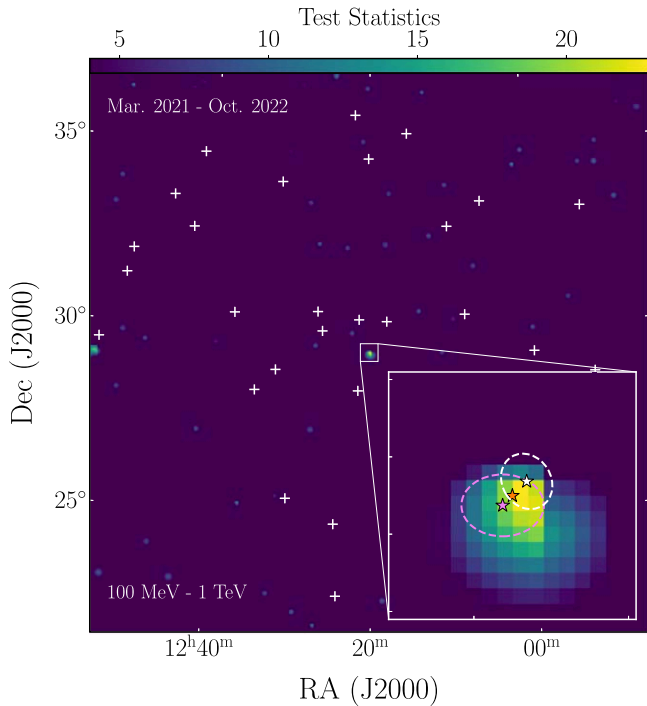


Figure 1. TS map of NGC 4278. The position of the 4FGL-DR4 sources (J. Ballet et al. 2023) are shown as white crosses. In the zoomed-in map, the orange star marks the radio position of NGC 4278 (C. Ly et al. 2004), while the violet and white stars are the LHAASO (Z. Cao et al. 2024a, 2024b) and Fermi-LAT best-fit positions, respectively. The LHAASO and Fermi-LAT 95% localization uncertainty regions are shown as dashed circular regions using the same color code.

We also checked the quality for the reconstructed events. All three event tracks in the detector are well tracked, and the reconstruction of the incoming direction is precise: the events at 8.2 and 102.5 GeV belong to PSF2, while the event at 95.5 GeV belongs to PSF3. The reconstructed arrival direction of each event is listed in columns (3) (R.A.) and (4) (decl.) in Table 1. Furthermore, we inspected the event class associated with each of the three photons. All of the events pass the CLEAN quality cut. The two VHE photons even belong to the SOURCEVETO class (see column (5) in Table 1). The associated classes exclude with very high probability that the detected photons are due to the residual background (see P. Bruel et al. 2018 for further details).

As a final test, the analysis was repeated selecting only events belonging to the purer CLEAN and SOURCEVETO classes, respectively. The results are completely consistent with the previous ones.

We computed the Fermi-LAT spectral energy distribution (SED) of the source using the `gta.sed` tool. This tool extracts the spectral data points of the given source by performing independent fits for the flux normalization in bins of energy. In each bin, we assumed a power-law model with a photon index fixed to the best-fit value ($\Gamma = 1.3$).

In Figure 2, the Fermi-LAT data points are shown as blue squares. If $TS < 9$, 3σ frequentist upper limits are reported as blue downward arrows.

Finally, we also comment on our results in comparison with ones from the literature (Z. Cao et al. 2024b; J.-S. Lian et al. 2024; Z.-R. Wang et al. 2024). Given the faintness of the source, a crucial aspect for the identification of enhanced γ -ray

activity from NGC 4278 is the choice of the time interval for the analysis. Z.-R. Wang et al. (2024) and J.-S. Lian et al. (2024) also analyzed Fermi-LAT data simultaneous to the period covered by the first LHAASO catalog (Z. Cao et al. 2024a). Standard analyses, similar to the ones performed by Z.-R. Wang et al. (2024) and J.-S. Lian et al. (2024), are suitable for sufficiently bright γ -ray sources, but not for weak sources such as NGC 4278, even when in flare. Indeed, the LHAASO collaboration extended the analysis of Fermi-LAT data until 2023 October 31 (Z. Cao et al. 2024b). The standard analysis techniques adopted also did not lead to any statistically significant detection in this case. A more complex, highly refined analysis, such as the one we described above, was crucial to achieve the best sensitivity of the LAT telescope, hence to reveal a statistically significant γ -ray emission from NGC 4278 in the selected period.

4. X-Ray Observations during the LHAASO Campaign

NGC 4278 has been extensively studied in the X-ray band. Thanks to its proximity, Chandra (M. C. Weisskopf et al. 2000; M. C. Weisskopf et al. 2002) could resolve both the nuclear and galactic emissions (N. J. Brassington et al. 2009; G. Fabiano et al. 2010; G. Younes et al. 2010). As shown by P12, the nucleus of this source is generally dominant and highly variable, with flux variations by a factor of ~ 18 from 2004 to 2010 in the 0.5–8 keV band.

No other pointings of the source are available in the public archives. Only Swift X-Ray Telescope (XRT; D. N. Burrows et al. 2000; J. E. Hill et al. 2000) serendipitously observed NGC 4278 for about 1 ks, on 2021 November 28, within the first LHAASO campaign. The online tool for Swift-XRT (see P. A. Evans et al. 2009 for details) was used to analyze these data. Swift-XRT has a limited angular resolution ($\sim 18''$ at 1.5 keV) with respect to Chandra-ACIS ($\sim 0''.5$ at 1.5 keV) that prevented us from performing a spatially resolved analysis. However, taking advantage of the detailed Chandra analysis by P12, we estimated the contribution to the X-ray spectrum from all the components (central AGN, LMXBs, thermal gas, etc.) falling within an area with a radius of $35''.4$ centered on the source, corresponding to the Swift-XRT extraction region. The total number of counts was 27, so we adopted the C-statistics (W. Cash 1979) and rebinned the data to have one count per energy bin. We allowed only the power-law parameters to vary and kept the spectral parameters and fluxes of the other components constant. We did not consider the contribution of unresolved AB+CV stars because it is negligible (see Figure 7 in P12). The intrinsic absorption was fixed to $N_H = 4 \times 10^{20} \text{ cm}^{-2}$ (P12).

Adopting the Levenberg–Marquardt minimization technique (J. A. Nousek & D. R. Shue 1989), the best fit resulted in a nuclear spectral slope of $\Gamma = 1.4^{+0.6}_{-0.6}$ and an unabsorbed flux of $\mathcal{F}_{0.5-8 \text{ keV}} = 5^{+3}_{-2} \times 10^{-12} \text{ erg s}^{-1} \text{ cm}^{-2}$ corresponding to a luminosity $\mathcal{L}_{0.5-8 \text{ keV}} = 1.6^{+0.9}_{-0.6} \times 10^{41} \text{ erg s}^{-1}$.

The Swift-XRT observation shows that the source was in a high state, with a flux comparable to the highest nuclear levels recorded by Chandra (P12).

5. Discussion and Conclusions

In this Letter, we report a 4.3σ Fermi-LAT detection of the low-luminosity radio galaxy NGC 4278, recently detected in the TeV

Table 1.
Properties of Photons Associated with NGC 4278 with a Probability Higher than 90%

| Energy (GeV) (1) | MJD (2) | α_{J2000} (deg) (3) | δ_{J2000} (deg) (4) | evclass (5) | gtsrcprob (%) (6) |
|------------------------|------------|----------------------------------|----------------------------------|----------------|-------------------------|
| 8.2 | 59561.1 | 184.9844 | 29.3550 | CLEAN | 93.8 (3.8, 2.1) |
| 95.5 | 59312.4 | 185.0258 | 29.2832 | SOURCEVETO | 99.9 (<1, <1) |
| 102.5 | 59561.1 | 184.9512 | 29.1962 | SOURCEVETO | 99.2 (<1, <1) |

Note. Column (1): reconstructed energy; column (2): arrival time in Modified Julian Date (MJD); columns (3)–(4): reconstructed R.A. and decl.; column (5): event class of the reconstructed event (further details in the text); column (6): association probability using the `gtsrcprob` tool for NGC 4278 and for the backgrounds in parentheses (isotropic and Galactic, respectively).

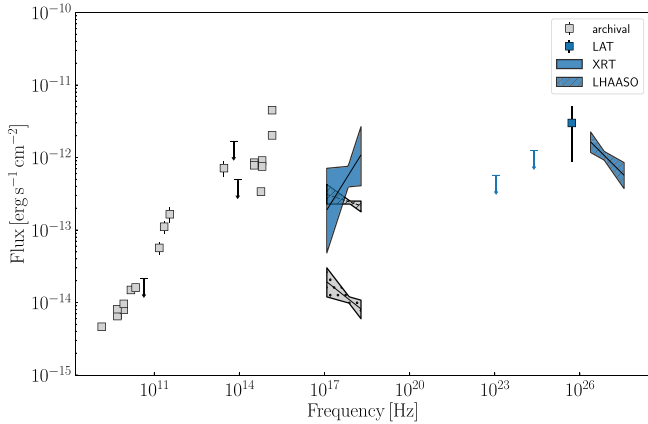


Figure 2. Multiwavelength and multipepoch SED of nuclear emission in NGC 4278. Archival data are shown in gray, and data are collected from I. W. A. Browne et al. (2004), M. Giroletti et al. (2005), A. Cardullo et al. (2009), G. Younes et al. (2010), S. Pellegrini et al. (2012), and J. W. Isbell et al. (2021). Swift-XRT, Fermi-LAT, and LHAASO simultaneous data are shown in blue and are from Z. Cao et al. (2024b) and this work.

band by LHAASO. We notice that NGC 4278 was included in the 1FLT catalog (L. Baldini et al. 2021) with a high probability ($P \sim 34\%$) of being a false positive. Therefore, we consider our result as the first solid detection of NGC 4278 in the GeV band.

It is likely that NGC 4278 periodically ejects relativistic plasma in the form of blobs (M. Giroletti et al. 2005). This hypothesis finds support in its radio spectrum, which shows a flattening below the peak frequency 1 GHz (S. E. Tremblay et al. 2016). The low-frequency radiation could be related to a radio relic, which remains after the old jets have dissipated their kinetic energy in the ISM. The total flux of NGC 4278 at 144 MHz recently reported by the Low-Frequency ARray (LOFAR; M. P. van Haarlem et al. 2013) Two-meter Sky Survey (LoTSS; T. W. Shimwell et al. 2017) is consistent with the flattening of the radio emission. Moreover, the LOFAR high-resolution ($6''$) image was fitted with more than a single Gaussian component, hinting potential extension of the source, possibly related to plasma located up to scales larger than ~ 500 pc. Chandra also provided further evidence. P12 noted that the gas in the innermost region (within 150 pc) is hotter than the ISM of the host galaxy. As suggested by the authors, this additional heating of the inner region may be due to the expansion of the jets in the ISM. The recent detection of NGC 4278 at TeV energy could represent a renewed activity of this source.

The Fermi-LAT detection of NGC 4278 and the high Swift-XRT X-ray flux during the LHAASO campaign provide further hints on the nuclear activity of this source. On the other hand, the large flux variations observed by Chandra suggest an origin

within the jet of the observed high-energy emission, possibly related to some form of jet perturbation (e.g., the injection of a new component in the ejection flow or an internal shock).

In Figure 2, we show the multiwavelength and multipepoch SED of the nuclear emission in NGC 4278. It is notable how the Fermi-LAT data seem to naturally extrapolate the TeV spectrum, showing a peak at $\sim 10^{26}$ Hz. This spectral feature resembles the high-energy bump often associated with inverse Compton radiation from jets in a leptonic scenario. However, the Swift-XRT X-ray emission does not connect smoothly with the Fermi-LAT data (see Figure 2). Its extrapolation to higher energies lies above the Fermi-LAT upper limits. This could indicate a synchrotron origin of the keV radiation, probably peaking in the hard X-ray band ($\gtrsim 10^{18}$ Hz; D. E. Harris & H. Krawczynski 2006; M. Georganopoulos et al. 2016) and resembling high-synchrotron-peaked BL Lac SEDs (see, e.g., G. Ghisellini et al. 2017).

Although a synchrotron self-Compton one-zone model is promising for fitting the Swift-XRT, Fermi-LAT, and LHAASO data of NGC 4278, it seems to falter when extended below 10^{17} Hz (see Figure 2). The lower-energy SED appears apart from and unrelated to the high-energy emission. Similar conclusions, although based on a slightly different data set of NGC 4278, were reached by J.-S. Lian et al. (2024) and S. Dutta & N. Gupta (2024). The low-energy SED, constructed from nonsimultaneous data found in the literature, likely represents the average state of NGC 4278's nucleus. Therefore, it is reasonable to hypothesize the higher-energy data as evidence of a transient, highly energetic event occurring during the LHAASO campaign.

Unfortunately, high angular resolution radio observations of the source during and after the LHAASO campaign are not currently available in the literature. To support the proposed picture, new radio observations are mandatory to ascertain potential radio structure perturbations.





In conclusion, the first detection of NGC 4278 at GeV and TeV energies paves the way to studying a new population of radio galaxies similar to high-frequency-peaked BL Lacs at high energies. This discovery demonstrates that even low-power objects can accelerate particles up to TeV energies, opening a new field of investigation for the Cherenkov Telescope Array Observatory (Cherenkov Telescope Array Consortium et al. 2019; R. Zanin et al. 2022).

Acknowledgments

The authors thank B. Rani, F. Longo, M. Kerr, and M. A. Sánchez-Conde for the useful suggestions that improved the clarity of this manuscript. The authors also thank L. Bruno, P. Da Vela, R. De Menezes, G. Migliori, C. Pallanca, and V. Sguera for intensive and constructive discussions. E.B. acknowledges financial support from the European Union—Next Generation

EU RFF M4C2 under the project IR0000012—CTA+ (CUP C53C22000430006), announcement N.3264 on 28/12/2021: “Rafforzamento e creazione di IR nell'ambito del Piano Nazionale di Ripresa e Resilienza (PNRR).” This work was supported by the European Research Council, ERC Starting grant MessMapp, S.B. Principal Investigator, under contract No. 949555, and by the German Science Foundation DFG, research grant “Relativistic Jets in Active Galaxies” (FOR 5195, grant No. 443220636). The Fermi-LAT Collaboration acknowledges support for LAT development, operation, and data analysis from NASA and DOE (United States), CEA/Irfu and IN2P3/CNRS (France), ASI and INFN (Italy), MEXT, KEK, and JAXA (Japan), and the K.A. Wallenberg Foundation, the Swedish Research Council and the National Space Board (Sweden). Science analysis support in the operations phase from INAF (Italy) and CNES (France) is also gratefully acknowledged. This work performed in part under DOE Contract DE-AC02-76SF00515.

ORCID iDs

Ettore Bronzini  <https://orcid.org/0000-0001-8378-4303>
 Paola Grandi  <https://orcid.org/0000-0003-1848-6013>
 Eleonora Torresi  <https://orcid.org/0000-0002-5201-010X>
 Sara Buson  <https://orcid.org/0000-0002-3308-324X>

References

- Abdollahi, S., Acero, F., Baldini, L., et al. 2022, *ApJS*, **260**, 53
- Antón, S., Browne, I. W. A., Marchã, M. J. M., Bondi, M., & Polatidis, A. 2004, *MNRAS*, **352**, 673
- Atwood, W., Albert, A., Baldini, L., et al. 2013, arXiv:1303.3514
- Atwood, W. B., Abdo, A. A., Ackermann, M., et al. 2009, *ApJ*, **697**, 1071
- Baldini, L., Ballet, J., Bastieri, D., et al. 2021, *ApJS*, **256**, 13
- Ballet, J., Bruel, P., Burnett, T. H., Lott, B., & The Fermi-LAT collaboration 2023, arXiv:2307.12546
- Balmaverde, B., & Capetti, A. 2014, *A&A*, **563**, A119
- Baum, S. A., O’Dea, C. P., Murphy, D. W., & de Bruyn, A. G. 1990, *A&A*, **232**, 19
- Bicknell, G. V., Mukherjee, D., Wagner, A. Y., Sutherland, R. S., & Nesvadba, N. P. H. 2018, *MNRAS*, **475**, 3493
- Brassington, N. J., Fabbiano, G., Kim, D. W., et al. 2009, *ApJS*, **181**, 605
- Bruel, P., Burnett, T. H., Digel, S. W., et al. 2018, arXiv:1810.11394
- Burrows, D. N., Hill, J. E., Nousek, J. A., et al. 2000, *Proc. SPIE*, **4140**, 64
- Callingham, J. R., Gaensler, B. M., Ekers, R. D., et al. 2015, *ApJ*, **809**, 168
- Cao, Z., Aharonian, F., An, Q., et al. 2024a, *ApJS*, **271**, 25
- Cao, Z., Aharonian, F., An, Q., et al. 2024b, *ApJL*, **971**, L45
- Cao, Z., della Volpe, D., Liu, S., et al. 2019, arXiv:1905.02773
- Capetti, A., de Ruiter, H. R., Fanti, R., et al. 2000, *A&A*, **362**, 871
- Cardullo, A., Corsini, E. M., Beifiori, A., et al. 2009, *A&A*, **508**, 641
- Cash, W. 1979, *ApJ*, **228**, 939
- Cherenkov Telescope Array Consortium, Acharya, B. S., Agudo, I., et al. 2019, in *Science with the Cherenkov Telescope Array*, ed. CTA Consortium (Singapore: World Scientific)
- Chiaberge, M., Capetti, A., & Macchetto, F. D. 2005, *ApJ*, **625**, 716
- Czerny, B., Siemiginowska, A., Janiuk, A., Nikiel-Wroczyński, B., & Stawarz, L. 2009, *ApJ*, **698**, 840
- De Young, D. S. 1991, *ApJ*, **371**, 69
- Dicken, D., Tadhunter, C., Axon, D., et al. 2012, *ApJ*, **745**, 172
- Dutta, S., & Gupta, N. 2024, *ApJ*, **974**, 56
- Evans, P. A., Beardmore, A. P., Page, K. L., et al. 2009, *MNRAS*, **397**, 1177
- Fabbiano, G., Brassington, N. J., Lentati, L., et al. 2010, *ApJ*, **725**, 1824
- Fanti, C., Fanti, R., Dallacasa, D., et al. 1995, *A&A*, **302**, 317
- Garcia, A. M. 1993, *A&AS*, **100**, 47
- Georganopoulos, M., Meyer, E. T., & Perlman, E. S. 2016, *Galax*, **4**, 65
- Ghisellini, G., Righi, C., Costamante, L., & Tavecchio, F. 2017, *MNRAS*, **469**, 255
- Giochetti, M., Taylor, G. B., & Giovannini, G. 2005, *ApJ*, **622**, 178
- González-Martín, O., Masegosa, J., Márquez, I., Guainazzi, M., & Jiménez-Bailón, E. 2009, *A&A*, **506**, 1107
- Harris, D. E., & Krawczynski, H. 2006, *ARA&A*, **44**, 463
- Hernández-García, L., González-Martín, O., Márquez, I., & Masegosa, J. 2013, *A&A*, **556**, A47
- Hill, J. E., Zugger, M. E., Shoemaker, J., et al. 2000, *Proc. SPIE*, **4140**, 87
- Ho, L. C., Feigelson, E. D., Townsley, L. K., et al. 2001, *ApJL*, **549**, L51
- Ho, L. C., Filippenko, A. V., Sargent, W. L. W., & Peng, C. Y. 1997, *ApJS*, **112**, 391
- Isbell, J. W., Burtscher, L., Asmus, D., et al. 2021, *ApJ*, **910**, 104
- Ito, H., Kino, M., Kawakatu, N., & Yamada, S. 2011, *ApJ*, **730**, 120
- Kiehlmann, S., Lister, M. L., Readhead, A. C. S., et al. 2024, *ApJ*, **961**, 240
- Kino, M., & Asano, K. 2011, *MNRAS*, **412**, L20
- Kino, M., Ito, H., Kawakatu, N., & Orienti, M. 2013, *ApJ*, **764**, 134
- Kuntschner, H., Emsellem, E., Bacon, R., et al. 2010, *MNRAS*, **408**, 97
- Lian, J.-S., Li, J.-X., Hu, X.-K., et al. 2024, *ApJ*, **974**, 134
- Lister, M. L., Homan, D. C., Kovalev, Y. Y., et al. 2020, *ApJ*, **899**, 141
- Ly, C., Walker, R. C., & Wrobel, J. M. 2004, *AJ*, **127**, 119
- Maness, H. L., Taylor, G. B., Zavala, R. T., Peck, A. B., & Pollack, L. K. 2004, *ApJ*, **602**, 123
- Maoz, D., Nagar, N. M., Falcke, H., & Wilson, A. S. 2005, *ApJ*, **625**, 699
- Marecki, A., Barthel, P. D., Polatidis, A., & Owsianik, I. 2003, *PASA*, **20**, 16
- Mattox, J. R., Bertsch, D. L., Chiang, J., et al. 1996, *ApJ*, **461**, 396
- Migliori, G., Siemiginowska, A., Kelly, B. C., et al. 2014, *ApJ*, **780**, 165
- Migliori, G., Siemiginowska, A., Sobolewska, M., et al. 2016, *ApJL*, **821**, L31
- Mukherjee, D., Bicknell, G. V., Wagner, A. Y., Sutherland, R. S., & Silk, J. 2018, *MNRAS*, **479**, 5544
- Nagar, N. M., Falcke, H., Wilson, A. S., & Ulvestad, J. S. 2002, *A&A*, **392**, 53
- Napier, P. J., Bagri, D. S., Clark, B. G., et al. 1994, *IEEEP*, **82**, 658
- Nousek, J. A., & Shue, D. R. 1989, *ApJ*, **342**, 1207
- O’Dea, C. P., & Baum, S. A. 1997, *AJ*, **113**, 148
- O’Dea, C. P., Baum, S. A., & Stanghellini, C. 1991, *ApJ*, **380**, 66
- O’Dea, C. P., & Saikia, D. J. 2021, *A&ARv*, **29**, 3
- Orienti, M. 2016, *AN*, **337**, 917
- Orienti, M., & Dallacasa, D. 2008, *A&A*, **487**, 885
- Owsianik, I., & Conway, J. E. 1998, *A&A*, **337**, 69
- Owsianik, I., Conway, J. E., & Polatidis, A. G. 1998, *A&A*, **336**, L37
- Peck, A. B., & Taylor, G. B. 2000, *ApJ*, **534**, 90
- Pellegrini, S., Wang, J., Fabbiano, G., et al. 2012, *ApJ*, **758**, 94
- Planck Collaboration, Aghanim, N., Akrami, Y., et al. 2020, *A&A*, **641**, A6
- Principe, G., Migliori, G., Johnson, T. J., et al. 2020, *A&A*, **635**, A185
- Readhead, A. C. S., Ravi, V., Blandford, R. D., et al. 2024, *ApJ*, **961**, 242
- Readhead, A. C. S., Xu, W., Pearson, T. J., Wilkinson, P. N., & Polatidis, A. 1993, AAS Meeting Abstracts, **182**, 53.07
- Readhead, A. C. S., Xu, W., Pearson, T. J., Wilkinson, P. N., & Polatidis, A. G. 1994, in *Compact Extragalactic Radio Sources*, Proc. of the NRAO workshop, ed. J. A. Zensus & K. I. Kellermann (Green Bank, WV: National Radio Astronomy Observatory), **17**
- Shapiro, K. L., Falcón-Barroso, J., van de Ven, G., et al. 2010, *MNRAS*, **402**, 2140
- Shimwell, T. W., Röttgering, H. J. A., Best, P. N., et al. 2017, *A&A*, **598**, A104
- Snellen, I. A. G., Schilizzi, R. T., Miley, G. K., et al. 2000, *MNRAS*, **319**, 445
- Stanghellini, C. 2003, *PASA*, **20**, 118
- Stanghellini, C., O’Dea, C. P., Dallacasa, D., et al. 2005, *A&A*, **443**, 891
- Stawarz, L., Ostorero, L., Begelman, M. C., et al. 2008, *ApJ*, **680**, 911
- Sutherland, R. S., & Bicknell, G. V. 2007, *ApSS*, **311**, 293
- Taylor, G. B., Charlot, P., Vermeulen, R. C., & Pradel, N. 2009, *ApJ*, **698**, 1282
- Taylor, G. B., Wrobel, J. M., & Vermeulen, R. C. 1998, *ApJ*, **498**, 619
- Terashima, Y., & Wilson, A. S. 2003, *ApJ*, **583**, 145
- Tingay, S. J., Macquart, J. P., Collier, J. D., et al. 2015, *AJ*, **149**, 74
- Tonry, J. L., Dressler, A., Blakeslee, J. P., et al. 2001, *ApJ*, **546**, 681
- Tremblay, S. E., Taylor, G. B., Ortiz, A. A., et al. 2016, *MNRAS*, **459**, 820
- Tschager, W., Schilizzi, R. T., Röttgering, H. J. A., Snellen, I. A. G., & Miley, G. K. 2000, *A&A*, **360**, 887
- van Breugel, W., Miley, G., & Heckman, T. 1984, *AJ*, **89**, 5
- van Haarlem, M. P., Wise, M. W., Gunst, A. W., et al. 2013, *A&A*, **556**, A2
- Wagner, A. Y., & Bicknell, G. V. 2011, *ApJ*, **728**, 29
- Wang, T.-G., & Zhang, X.-G. 2003, *MNRAS*, **340**, 793
- Wang, Z.-R., Xue, R., Xiong, D., et al. 2024, *ApJS*, **271**, 10
- Weisskopf, M. C., Brinkman, B., Canizares, C., et al. 2002, *PASP*, **114**, 1
- Weisskopf, M. C., Tananbaum, H. D., Van Speybroeck, L. P., & O’Dell, S. L. 2000, *Proc. SPIE*, **4012**, 2
- Wilkinson, P. N., Polatidis, A. G., Readhead, A. C. S., Xu, W., & Pearson, T. J. 1994, *ApJL*, **432**, L87
- Wilks, S. S. 1938, *Annals Math. Statist.*, **9**, 60
- Wood, M., Caputo, R., Charles, E., et al. 2017, *ICRC (Busan)*, **301**, 824
- Younes, G., Porquet, D., Sabra, B., et al. 2010, *A&A*, **517**, A33
- Zanin, R., Abdalla, H., Abe, H., et al. 2022, *ICRC (Berlin)*, **37**, 5